Available online at www.sciencedirect.com
SCIENCE DIRECT®
PERGAMON
Polyhedron 22 (2003) 2363–2374
POLYHEDRON
www.elsevier.com/locate/poly

Coordination complexes of a silicon-linked organic tetranitroxide

Martha Baskett [a], Paul M. Lahti [a,*], Fernando Palacio [b]

[a] Department of Chemistry, University of Massachusetts, 701 Lederle GRT A 710 North Pleasant Street, Amherst, MA 01003, USA
[b] Instituto de Ciencia de Materiales de Aragón, CSIC-Universidad de Zaragoza, 50009 Zaragoza, Spain

Received 9 October 2002; accepted 1 February 2003

Abstract

Two 1:1 coordination polymers were synthesized linking tetraradical tetrakis(*N*-oxyl-2,2,6,6-tetramethylpiperidin-4-oxyl)silane, (**3**) and M(hfac)$_2$ (M = Mn, Cu). Both are 1-D systems in which two TEMPO sites remain uncoordinated: Mn(hfac)$_2$(**3**) = **4** and Cu(hfac)$_2$(**3**) = **5**. System **4** has strong AFM TEMPO–Mn–TEMPO exchange even at room temperature (a net $S = 3/2$ spin unit), with the remaining two TEMPO units in each monomer acting in an essentially isolated manner. System **4** shows FM exchange within the TEMPO–Cu–TEMPO trimer unit, with an increase in magnetization up to a broad maximum at about 16–20 K before decreasing again due to likely antiferromagnetic interactions between trimers. The magnetic susceptibility data up to the maximum point can be fit to an FM coupled three-spin model with two additional noninteracting spins, yielding J/k (TEMPO–Cu–TEMPO) $\cong (+)89$ K. The low temperature AFM interactions observed for **4**–**5** are attributed to interchain spin pairing.

Keywords: Coordination polymers; TEMPO; Nitroxides; Copper(II) complexes; Manganese(II) complexes

1. Introduction

The coordination of organic nitroxides with paramagnetic transition metal cations has been a successful means of creating new molecular magnetic materials with varying dimensionality. Efforts to increase the ordering temperatures of various members of this family of materials have focused on creating new three-dimensional (3-D) motifs for the coordination, and upon improving the exchange interaction strength between the spin bearing units in the material.

We recently reported the synthesis of silicon-centered tetraradical **1** [1], a potential organic linker unit for 3-D networks with metal cations (Scheme 1). A recent report by Mathevet and Luneau describes such a 3-D coordination net, using the carbon-centered tetraradical **2** [3]. This system showed strong antiferromagnetic (AFM) exchange between Mn(II) ions and coordinated nitroxide radicals in the 60–300 K region, with weak AFM coupling between spin sites at temperatures below 60 K. However, there was no longer-range spin-ordering. We hoped that use of a central silicon atom would assist 3-D exchange through a tetrahedral center, possibly due in part to d-orbital participation.

Despite numerous efforts, we so far have not been able to make complexes of **1** as single crystalline materials. In an effort to model the desired complexes, we coordinated the non-conjugated, silicon-centered tetraradical **3** (TETRA) with Mn(hfac)$_2$ and Cu(hfac)$_2$.

2. Experimental

2.1. Synthesis

Previously known [4] tetraradical **3** was synthesized by the method of Gruzinova et al. [4d] from silicon tetrachloride and commercially available 4-hydroxy-TEMPO. The final red tetraradical appears to be indefinitely stable in air. Like previous workers [4a,4b,4c], we found the room temperature solution phase electron spin resonance (ESR) spectrum to give a nonet pattern with a peak-to-peak splitting of 3.97 G, indicating that the inter-spin exchange energy is significantly larger than the nitrogen hyperfine coupling on

* Corresponding author. Tel.: +1-413-545-4890; fax: +1-413-545-4490.
E-mail address: lahti@chem.umass.edu (P.M. Lahti).

0277-5387/03/$ - see front matter © 2003 Elsevier Science Ltd. All rights reserved.
doi:10.1016/S0277-5387(03)00300-0

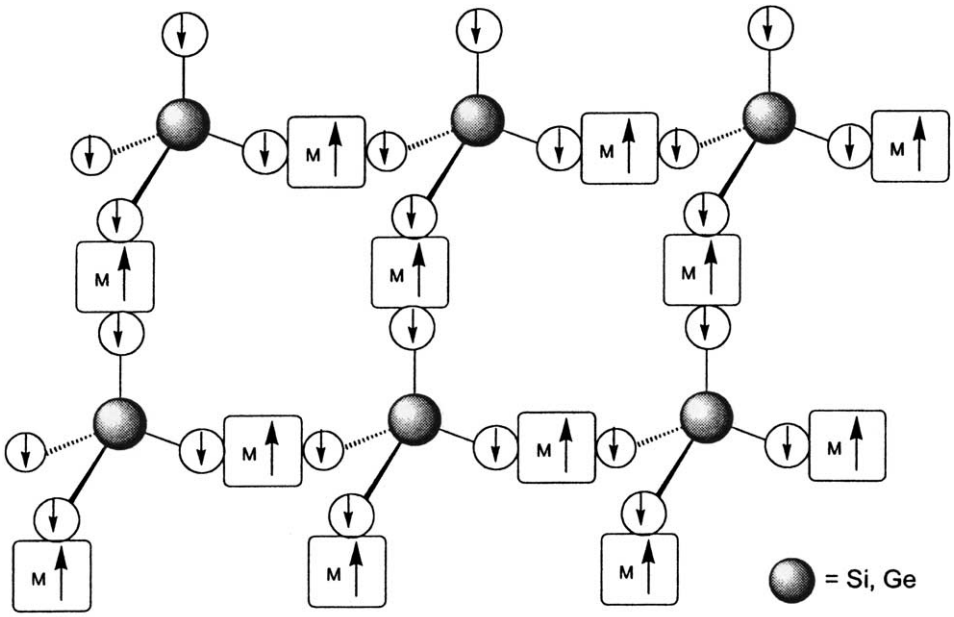

A Possible 3-D Net Linking Tetraradicals and Paramagnetic Cations.

Scheme 1.

the nitroxides (J/k(NO···NO)···a_N). The magnetic behavior of neat solid **3** has been reported by Nakajima et al. [4c], and interpreted in terms of spin-cluster formation at lower temperatures; it is not clear whether the spin clusters are formed in an intra- or intermolecular fashion. We published a crystal structure of **3** in an earlier [2] communication. We have now found that **3** can form two polymorphs, the monoclinic form that we first described, and an orthorhombic form that is more frequently formed. The allotropes have similar molecular structures, save for one dihedral Si–O–TEMPO angle (see the discussion in the crystallography section).

Tetraradical **3** was mixed in various ratios with the hfac salts of Mn(II) and Cu(II) in hexanes (Fig. 1), after azeotropic removal of the water of hydration from the inorganic solutions. Slow crystallization led to the formation of 1:1 complexes **4**–**5**, 1-D coordination polymers in which two TEMPO groups of **3** are coordinated, and two are not. Despite a number of attempts, we have not obtained complexes of **3** that have more than two TEMPO groups coordinated [5].

The structures of **4**–**5** were verified by X-ray crystallography. Although the manganese complex **4** gave stable, good quality crystals, it was difficult to grow single crystals of **5** of sufficient quality to give high-grade refinement. Complex **5** also discolors upon exposure to light so we did all analyses as quickly as possible after initial synthesis.

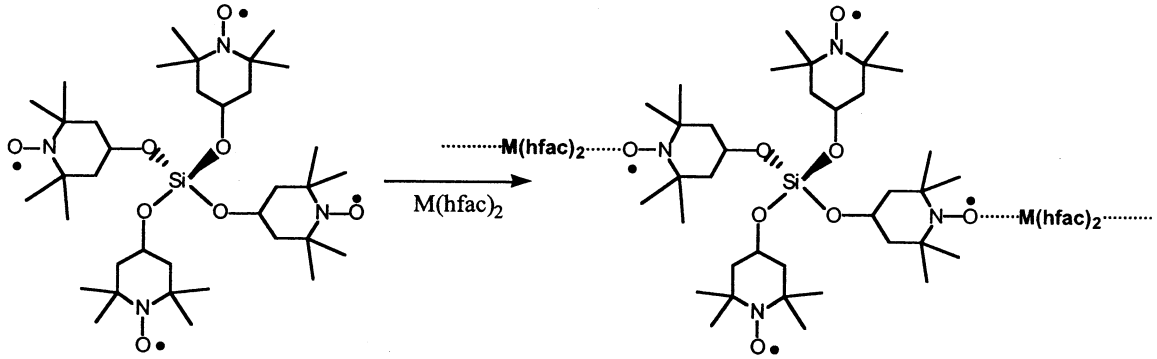

3

4 M = Mn
5 M = Cu

Fig. 1. Synthetic route to make **4**–**5**.

2.1.1. Tetrakis(N-oxyl-2,2,6,6-tetramethylpiperidin-4-oxyl)silane (3, TETRA)

Freshly distilled pyridine (190 μl, 2.32 mmol) was added via syringe to a stirring solution of 4-hydroxy-2,2,6,6-tetramethylpiperidinoxy (Aldrich, 0.40 g, 2.32 mmol) in dry ether (10 ml) at 0 °C under argon. A solution of silicon tetrachloride (0.09 g, 0.581 mmol) in dry ether (2 ml) was placed under argon in a small addition funnel and added dropwise to the stirring solution over 25 min. The mixture was allowed to warm slowly to room temperature over 8 h, and stirred for a further 12 h. The resulting mixture was filtered through Celite. The filtrate was concentrated under vacuum to afford 0.26 g of red oil (62%), which was recrystallized from hexanes to give blocky red crystals. The melting point sometimes varied with the preparation and number of recrystallizations, although TLC and elemental analysis indicated a high level of purity. We attribute this to occasional formation of mixtures of allotropes. The literature melting point is 160–165 °C [4a] Anal. Calc. for $C_{36}H_{68}N_4O_8Si$: C, 60.64; H, 9.61; N, 7.86; O, 17.95; Si, 3.94. Found: C, 60.83; H, 9.77; N, 7.65%. ESR (2-methyltetrahydrofuran, room temp, 9.630 GHz, 100 kHz modulation frequency, 1.01 G modulation amplitude): nonet ($\Delta H_{pp} = 3.97$ G).

2.1.2. Manganese(II)-bis(hfac)-tetrakis(N-oxyl-2,2,6,6-tetramethylpiperidin-4-oxyl)silane (4, Mn(hfac)$_2$TETRA)

$Mn(hfac)_2 \cdot 2H_2O$ (9.38 mg, 0.02 mmol) was dissolved in 0.5 ml of ether. Hexane (38 ml) was added, and water was azeotropically removed along with 18 ml of solvent in a Dean–Stark apparatus under argon. Compound **3** (7.13 mg, 0.01 mmol) was placed in a 50 ml round bottom flask and dissolved in 3 ml of warm hexane. The flask was placed under argon, and the cooled $Mn(hfac)_2$ solution was introduced via syringe. After three days, small red crystals formed in the colorless, clear solvent; these were isolated by filtration and dried under vacuum to give **4**, m.p. 194–196 °C. Anal. Calc. for $C_{46}H_{70}F_{12}MnN_4O_{12}Si$: C, 46.74; H, 5.97; N, 4.74. Found: C, 46.72; H, 6.07; N, 4.69%. The structure was confirmed using X-ray crystallography (see below).

2.1.3. Copper(II)-bis(hfac)-tetrakis(N-oxyl-2,2,6,6-tetramethylpiperidin-4-oxyl)silane (5, Cu(hfac)$_2$TETRA)

Compound **3** (7.13 mg, 0.01 mmol) was dissolved in ether (1 ml) and dichloromethane (2 drops) in a 20 ml vial. $Cu(hfac)_2 \cdot xH_2O$ (9.9 mg, 0.02 mmol) was added along with heptane (10 ml). Small light green crystals precipitated the next day from colorless supernatant solvent. The solid **5** was isolated by filtration and drying under argon (m.p. 163–164 °C), and stored in a −30 °C freezer in the dark to limit discoloration that occurs upon standing. Anal. Calc. for $C_{46}H_{70}CuF_{12}N_4O_{12}Si$: C, 46.40; H, 5.93; N, 4.71. Found: C, 46.20; H, 6.03; N, 4.97. The structure was confirmed using X-ray crystallography (see below).

2.2. Crystallography

All crystallographic analyses were carried out by A. Chandrasekaran of the UMass-Amherst X-ray Structural Characterization Center (NSF CHE-9974648). Summaries of the analyses are given in Table 1.

2.2.1. Tetrakis(N-oxyl-2,2,6,6-tetramethylpiperidin-4-oxyl)silane (3-α, TETRA-monoclinic)

Analysis was carried out on a Bruker P4 at ambient temperature with Mo Kα radiation, $\lambda = 0.7107$ Å, μ(Mo Kα) = 0.104 mm^{-1}. Ruby red block 0.55 × 0.55 × 0.55 mm, m.p. 126–128 °C, monoclinic, $P\bar{1}$ (#2), $a = 19.0646(3)$, $b = 11.8693(2)$, $c = 19.1899(3)$ Å, $\beta = 100.5005(11)°$, $Z = 4$, $V = 4269.64(12)$ Å^3, $D_{calc} = 1.109$ g cm^{-3}. $N = 7471$ unique reflections were measured using ω scans for $4.10 < \theta < 25.05°$. The structure was solved by direct methods and refined on F^2 for all reflections with $I > 2\sigma(I)$ using 442 parameters and full matrix least squares in SHELXL-97 [6] to yield the structure with $R_1 = 0.0562$, $wR_2 = 0.1347$. An ORTEP representation is given in Fig. 2.

2.2.2. Tetrakis(N-oxyl-2,2,6,6-tetramethylpiperidin-4-oxyl)silane (3-β, TETRA-orthorhombic)

Analysis was carried out on a Bruker P4 at ambient temperature with Mo Kα radiation, $\alpha = 0.7107$ Å, μ(Mo Kα) = 0.106 mm^{-1}. Red–orange block 0.75 × 0.50 × 0.25 mm, m.p. 153–154 °C, orthorhombic, *Fdd*2 (#43), $a = 42.9935(7)$, $b = 22.5193(4)$, $c = 8.63160(10)$, $Z = 8$, $V = 8357.0(2)$ Å^3, $D_{calc} = 1.133$ g cm^{-3}. $N = 3584$ unique reflections were measured using ω scans for $4.09° < \theta < 25.03°$. The structure was solved by direct methods and refined on F^2 for all reflections with $I > 2\sigma(I)$ using 223 parameters and full matrix least squares in SHELXL-97 [6] to yield the structure with $R_1 = 0.0364$, $wR_2 = 0.0834$. An ORTEP representation is given in Fig. 2.

2.2.3. Mn(hfac)$_2$TETRA (4)

Analysis was carried out on a Bruker P4 at ambient temperature with Mo Kα radiation, $\lambda = 0.7107$ Å, μ(Mo Kα) = 0.340 mm^{-1}. Opaque red block, 0.80 × 0.65 × 0.50 mm; monoclinic space group $P2_1/c$ (#14), with $a = 13.58290(10)$, $b = 38.3724(3)$, $c = 11.26830(10)$, $\beta = 90.7307(3)°$, $V = 5872.66(8)$ Å^3, $Z = 4$, $D_{calc} = 1.337$ g cm^{-3}. $N = 10\,002$ unique reflections were measured using ω scans for $4.11 < \theta < 25.03°$. The structure was solved by direct methods and refined on F^2 for all reflections with $I > 2\sigma(I)$ using 685 parameters and full matrix least squares in SHELXL-97 [6] to yield the structure with $R_1 = 0.0606$, $wR_2 = 0.1625$. The TEMPO–O–Si dihedral angle

Table 1
Crystallographic summary data for **3–5**

	3-α	**3**-α	**4**	**5**
Chemical formula	$C_{36}H_{68}N_4O_8Si$	$C_{36}H_{68}N_4O_8Si$	$C_{46}H_{70}F_{12}MnN_4O_{12}Si$	$C_{46}H_{70}CuF_{12}N_4O_{12}Si$
Chemical formula weight	713.03	713.03	1182.09	1190.69
Temperature	293	293	293	293
Cell setting, space group	Monoclinic, $P\bar{1}$	Orthorhombic, *Fdd*2	Monoclinic, $P2_1/c$	Monoclinic, $P2_1/c$
a (Å)	19.0646(3)	42.9935(7)	13.58290(10)	27.5606(3)
b (Å)	11.8693(2)	22.5193(4)	38.3724(3)	18.8054(2)
c (Å)	19.1899(3)	8.63160(10)	11.26830(10)	11.64810(10)
α (°)	90	90	90	90
β (°)	100.5005(11)	90	90.7307(3)	92.0487(4)
γ (°)	90	90	90	90
V (Å^3)	4269.64(12)	8357.0(2)	5872.66(8)	6033.21(10)
Z	4	8	4	4
D_x (Mg m^{-3})	1.109	1.133	1.337	1.311
Radiation type	Mo Kα	Mo Kα	Mo Kα	Mo Kα
θ Range (°)	4.08–25.03	4.09–25.03	4.11–25.03	4.08–25.02
F(000)	1560	3120	2468	7116
μ (mm^{-1})	0.104	0.106	0.340	0474
Crystal color	Red block	Red block	Deep purple needle	Deep purple needle
Data collection method	$\omega-2\theta$ scans	$\omega-2\theta$ scans	$\omega-2\theta$ scans	$\omega-2\theta$ scans
Collected/unique reflections	13 651/7471	3584/3584	18 347/10 002	20 503/10 550
Criterion for observed reflections	$I > 2\sigma(I)$	$I > 2\sigma(I)$	$I > 2\sigma(I)$	$I > 2\sigma(I)$
R_{int}	0.0266	0.0266	0.0213	0.0254
Range of *h,k,l*	$-22 \rightarrow h \rightarrow 22$	$-50 \rightarrow h \rightarrow 50$	$-16 \rightarrow h \rightarrow 16$	$-32 \rightarrow h \rightarrow 32$
	$-13 \rightarrow k \rightarrow 14$	$-25 \rightarrow k \rightarrow 26$	$-4 \rightarrow k \rightarrow 43$	$-22 \rightarrow k \rightarrow 22$
	$-22 \rightarrow l \rightarrow 22$	$-10 \rightarrow l \rightarrow 10$	$-1 \rightarrow l \rightarrow 13$	$-13 \rightarrow l \rightarrow 13$
Completeness to 2θ	0.99	0.99	0.96	0.99
Reflections, restraints, parameters	7471/0/442	3584/1/223	10 002/138/685	10 550/552/668
H-atom treatment	Mixed	Mixed	MIxed	Mixed
Goodness of fit on F^2	1.041	1.037	1.034	1.039
$\Delta\rho_{max}$, $\Delta\rho_{min}$ (e Å^{-3})	0.240, −0.243	0.116, −0.151	1.023, −0.540	0.983, −0.555
R_1, wR_2 ($I > 2\sigma(I)$)	0.0562, 0.1347	0.0364, 0.0777	0.0606, 0.1625	0.1074, 0.2978
R_1, wR_2 (all)	0.0881, 0.1569	0.0490, 0.0834	0.0697, 0.1703	0.1407, 0.3273
Program used	SHELXL-97	MAXUS	SHELXL-97	SHELXL-97

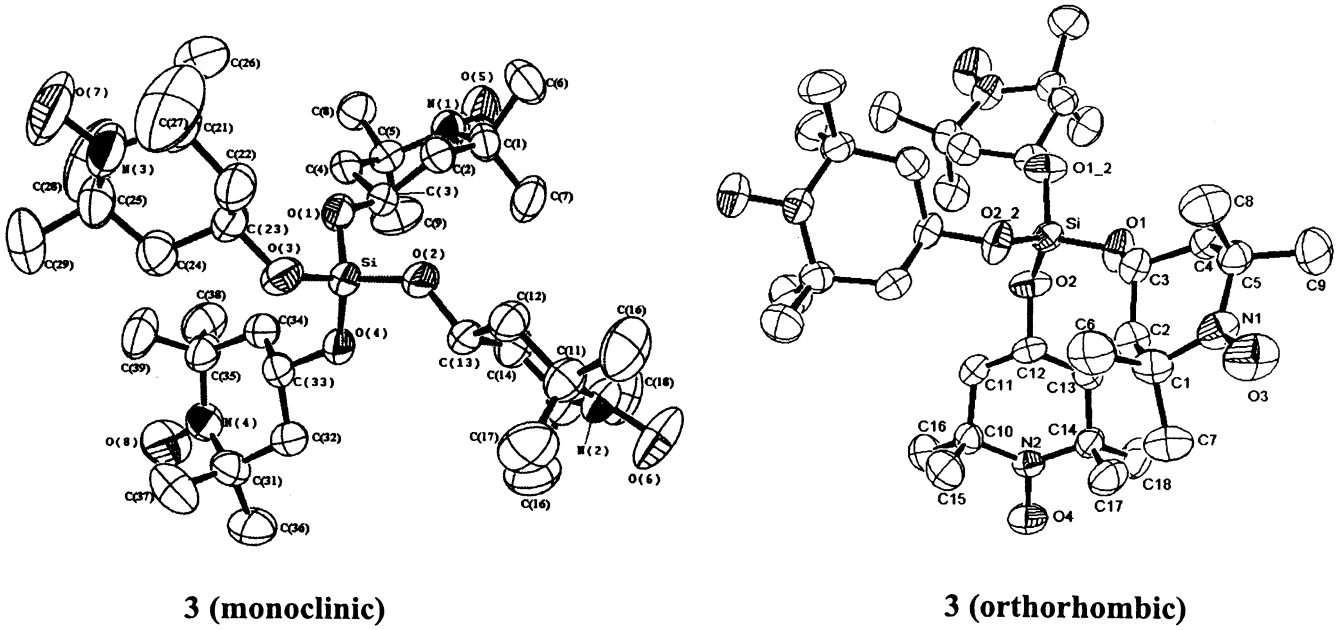

Fig. 2. Crystallographic numbering schemes for monoclinic and orthorhombic phases of **3**.

in the structure is disordered. The same crystal structure was obtained using 1:1, 1:2, 1:3 or 1:4 ratios of **3**:Mn(hfac)$_2$·2H$_2$O when the compounds were placed in an open container, dissolved in a small amount of ether or dichloromethane, and additional solvent (hexane, heptane or benzene) added. An ORTEP representation is given in Fig. 3.

2.2.4. *Cu(hfac)$_2$TETRA (**5**)*

Analysis was carried out on a Bruker P4 at ambient temperature with Mo Kα radiation, $\lambda = 0.7107$ Å, μ(Mo Kα) = 0.474 mm^{-1}. Opaque red block, 1.00 × 0.50 × 0.40 mm; monoclinic space group $P2_1/c$ (#14), with $a = 27.5606(3)$, $b = 18.8054(2)$, $c = 11.64810(10)$, $\beta = 92.0487(4)^\circ$, $V = 6033.21(10)$ Å^3, $Z = 4$, $D_{calc} = 1.311$ g cm^{-3}. $N = 10\,550$ unique reflections were measured using ω scans for $4.08 < \theta < 25.02^\circ$. The structure was solved by direct methods and refined on F^2 for all reflections with $I > 2\sigma(I)$ using 668 parameters and full matrix least squares in SHELXL-97 [6] to yield the structure with $R_1 = 0.1074$, $wR_2 = 0.2978$. Multiple efforts did not yield better refinement, possibly because of rapid decomposition (discoloration). An ORTEP representation is given in Fig. 4.

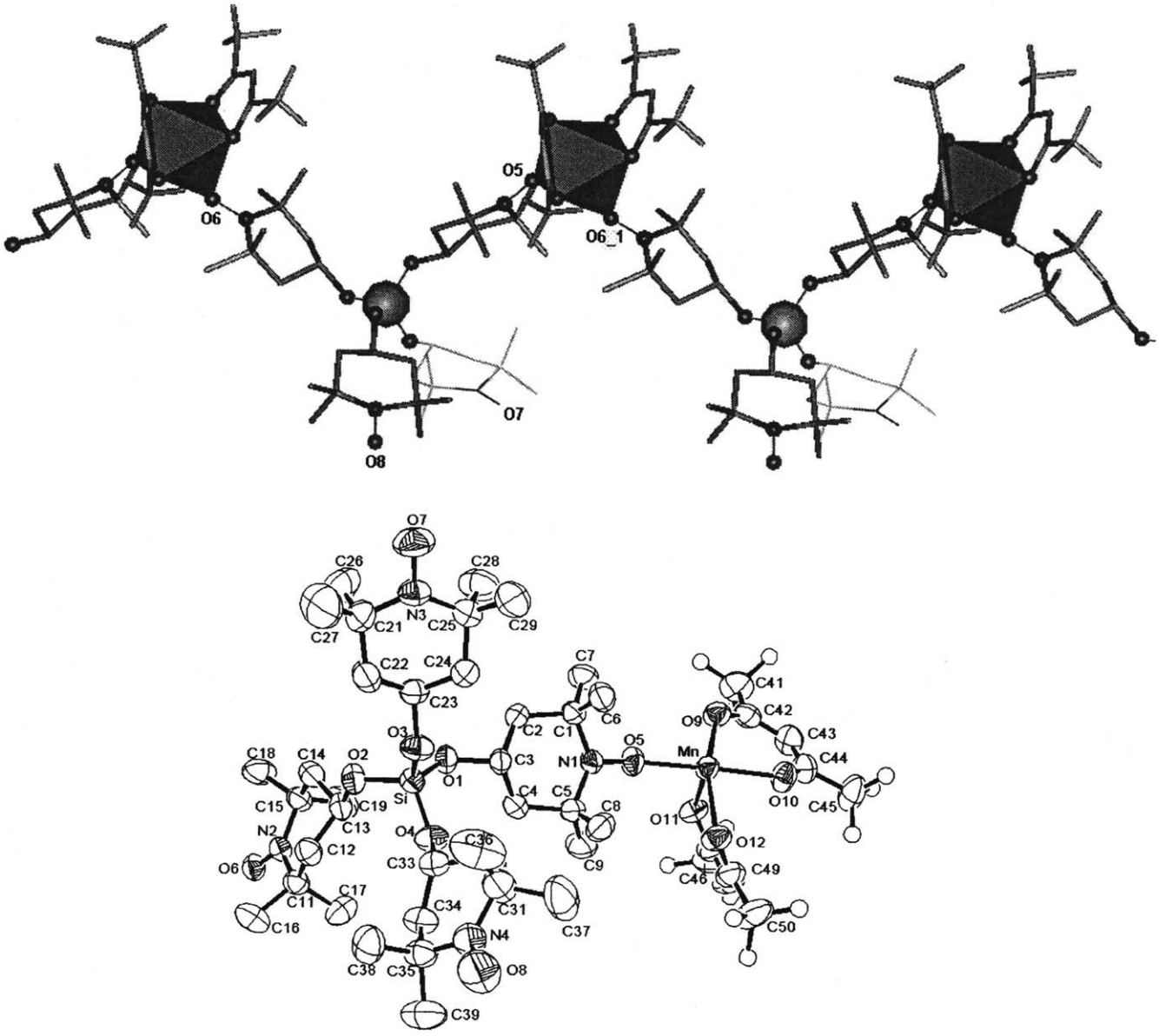

Fig. 3. Partial crystallographic numbering schemes for complex **4**. Fluorine atoms are shown as spheres instead of thermal ellipsoids for ease of viewing.

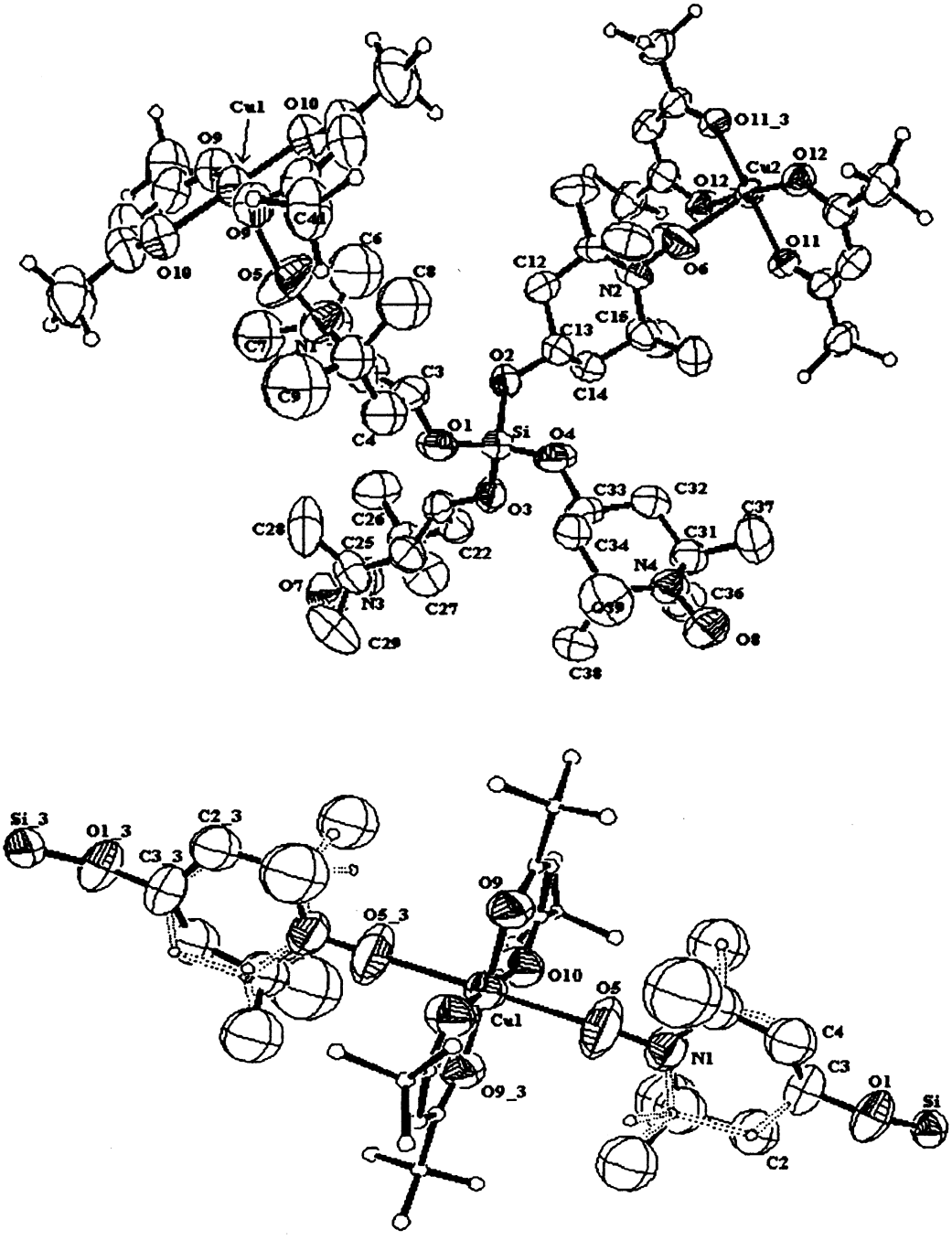

Fig. 4. Partial crystallographic numbering schemes for complex **5**. Fluorine atoms are shown as spheres instead of thermal ellipsoids for ease of viewing. Disorder in the TEMPO groups about the TEMPO–Cu(1)–TEMPO axis is shown by dashed/atoms bonds in the lower part of the figure.

2.3. Magnetic studies

Magnetization measurements for **4**–**5** were carried out on a Quantum Design MPMS SQUID magnetometer. Samples were placed in gelatin capsules and held in place with a small amount of cotton; before measurement, a helium purge procedure was carried out to avoid oxygen contamination. The magnetic susceptibility (χ) was analyzed at an external magnetic field of 1 T over a temperature range of 1.8–300 K. Magnetization (M) was also measured as a function of magnetic field (H) at 1.8 and 3.0 K. Final measurements were corrected for temperature independent terms and diamagnetism of the sample and sample holder. Fig. 5 shows plots of χT versus T and M versus H at 1.8 K for **4**. Fig. 6 shows the χT versus T data for **5**.

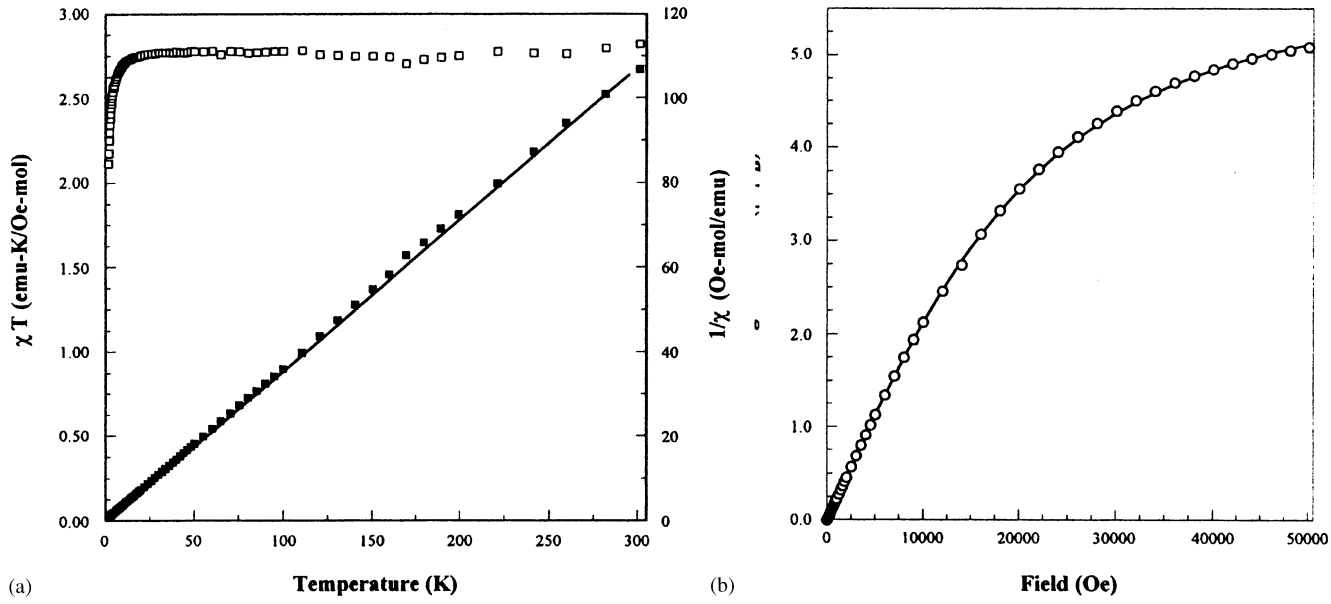

Fig. 5. Reciprocal magnetic susceptibility versus temperature ($1/\chi$ vs. T, ■) and χT vs. T (□) measurements at 10 kOe (a); magnetization (○) versus field (b) for **4**.

3. Results and discussion

3.1. Crystallography

As mentioned above, the molecular structures of the allotropes of **3** differ mainly in the dihedral angles formed by the Si–O–TEMPO linkages, as summarized in Table 2. The dihedral angles exhibited by **3** in complexes **4**–**5** are quite close to that in **3**-α, again supporting the idea that the two geometries seen in **3** are very close in energy. This is reasonable, given that the two forms are rotational isomers. These differences should not make any significant change in magnetic behavior, given the lack of a direct conjugation path

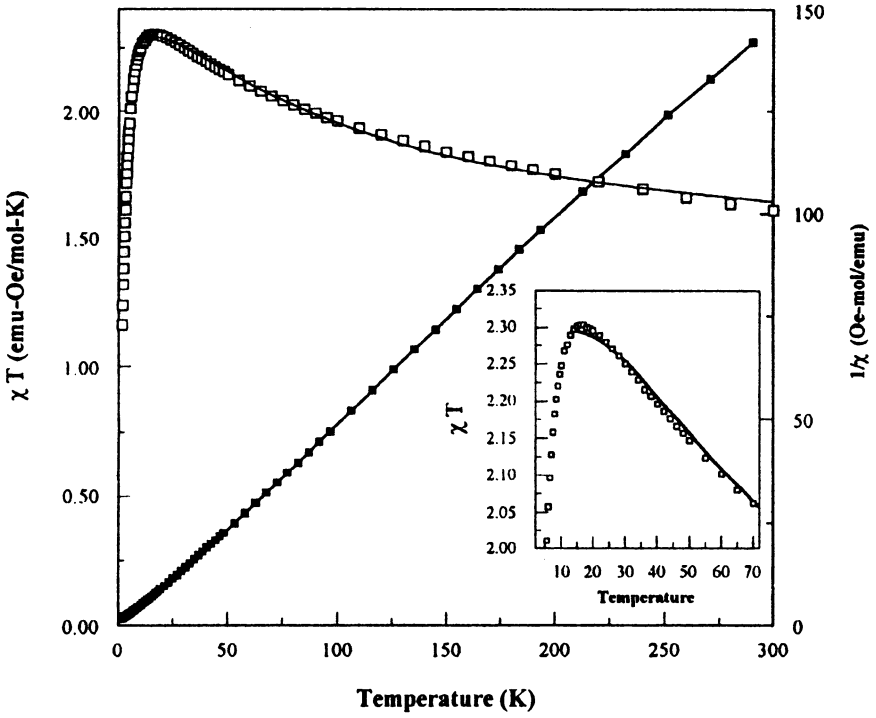

Fig. 6. Plots reciprocal magnetic susceptibility versus temperature ($1/\chi$ vs. T, ■) and χT vs. T (□) measurements at 10 kOe (a); magnetization versus field (b) for **5**. The fitted curve for the χT vs. T data uses Eq. (3) given in the text. Inset shows a blowup of the low temperature region for the data and the fitted curve.

Table 2
Comparisons of torsional bonding parameters for **3-α**, **3-β**, **4**, and **5**

3-α	**3-β**	**4**	**5**
5.1°	18.4°	4.5°	18.2°
Si–O(3)–C(23)H	Si–O(1)–C(3)H	Si–O(3)–C(23)H	Si–O(4)–C(33)H
23.4	18.4	23.4	34.4
Si–O(2)–C(13)H		Si–O(4)–C(33)H	Si–O(2)–C(13)H
26.3	32.5	22.2 [a]	25.8 [a]
Si–O(1)–C(3)H	Si–O(2)–C(12)H	Si–O(1)–C(3)H	Si–O(4)–C(33)H
44.2	32.5	13.3 [a]	49.5 [a] (3.1 [a,b])
Si–O(4)–C(33)H		Si–O(2)–C(13)H	Si–O(3)–C(23)H

All dihedrals measured as (H)C–O–Si linkage in (°). Clockwise/counterclockwise torsional convention is ignored, and only absolute values of torsion given.

[a] Nitroxide group is coordinated in the polymer chain.

[b] Alternate torsion due to disorder in nitroxide group.

between the nitroxide units, and substantial intramolecular NO···NO distances (> 10 Å).

Both of the complexes **4**–**5** are 1-D coordination polymers. In **4**, two TEMPO oxygens and two hfac oxygens (O(5), O(6), O(10), and O(11)) form an essentially square planar array around the central manganese ion. The remaining hfac ligation sites (O(9) and (O(12)) are significantly distorted relative to pseudo-octahedral position, forming an O(9)–Mn–O(12) angle of 155.2°, rather than the ideal 180°. Given the observed geometry of **4**, the TEMPO groups are either both equatorially coordinated, or may be one axial and one equatorial. Since the exchange behavior of the Mn–TEMPO linkage is not expected to depend upon axial or equatorial coordination, more detailed analysis of the coordination sphere in **4** is not magnetically crucial. By comparison, the copper atoms in **5** occupy inversion symmetry positions, with nitroxide oxygen atoms axially complexed at opposite vertices of a readily identified pseudo-octahedron (Fig. 4).

The Mn–O(TEMPO) bonds in **4** are 0.09–011 Å shorter than the Mn–O(hfac) bonds. The TETRA moieties (**3**) in the 1-D chain are conformationally almost identical to the monoclinic geometry [2] of **3**, based upon the Si–O–C–H dihedral angles formed by connection of the various TEMPO units in both **3** and **4** to the central silicon atom. The Cu–O(TEMPO) bonds in **5** are longer by almost 0.5 Å longer than the Cu–O(hfac) bonds. Both M–O(TEMPO) and M–O(hfac) bond lengths are typical by comparison to similar molecules [7].

The TEMPO groups coordinated to Cu(1) in **5** are disordered about an axis formed approximately by C(3)···N(1)–O(4)···Cu(1)···O(4)–N(1)···C(3) (Fig. 4). The position of the Cu(1)···O(5)N(1) (TEMPO) bond is not significantly affected. The disorder is an approximately 40° twist of one TEMPO group that leaves the main SiO_4 moiety and the nitroxide NO groups in place. The NO–Cu–ON linkage is almost the same in both twistomers.

Both coordination polymers stack in a sinusoidal pattern in a plane, due to the shape of the TETRA linker. The chains in **4** stack like corrugated sheets along the *a*-axis, with both uncoordinated TEMPO groups stacked in an alternating fashion and interdigitated between chains along the *c*-axis (Table 3, O(7)···O(7′) and O(8)···O(8′) contacts). Because of the linearizing nature of the TEMPO–Cu–TEMPO segments in **5**, the polymer repeat length is longer (27.56 Å) than in **4** (13.58 Å), but **5** also packs in a somewhat corrugated fashion. Uncoordinated TEMPO units in **5** also interdigitate along the *c*-axis (Table 3). There are CH···O type interactions in **4** between uncoordinated nitroxide oxygens and geminal methyl groups on a coordinated TEMPO of another chain; r[O(7)···C(18′)] = 3.659 Å and r[O(7)···C(19′)] = 3.861 Å for one TEMPO group, r[O(8)···C(8′)] = 3.734 Å and r[O(8)···C(9′)] = 3.765 Å for the other. In **5**, similar CH···O interactions occur between the NO group on an uncoordinated TEMPO unit and two axial methyl groups; r[O(8)···C(17′)] = 3.508 Å, r[O(8)···C(19′)] = 3.658 Å for one TEMPO group. Fig. 7 schematically shows a number of these interactions. We believe that these contacts help to link the chains together, even though we are not able to locate the hydrogen atom positions definitively in order to locate specific hydrogen-bond like contacts.

In **4**, the polymer chains propagate along the *b*-axis, in **5** along the *a*-axis. The 1-D chains in the polymers pack in a manner that does not bring the uncoordinated TEMPO groups into close proximity. The closest NO···ON contacts between uncomplexed TEMPO groups are 5.9–6.0 Å between the interdigitated, uncomplexed TEMPO groups in both **4** and **5** (Table 3). Interestingly, there are somewhat closer contacts between an uncomplexed TEMPO and a complexed TEMPO in both polymers: r[O(7)···O(5′)] = 4.74 Å in **4**, and r[O(8)···O(6′)] = 5.34 Å in **5**. These contacts

Table 3
Selected molecular and interatomic relationship parameters for **4–5**

4			
Mn–O(5)	2.089 [a] Å	O(7)···O(7′)	5.997 [b]
Mn–O(6)#	2.075 [a]	O(8)···O(8′)	6.018 [b]
Mn–O(9)	2.180	O(7)···O(5′)	4.743 [c]
Mn–O(10)	2.161	O(7)···O(6′)	6.099 [c]
Mn–O(11)	2.162	O(7)···C(18′)	3.659 [d]
Mn–O(12)	2.161	O(7)···C(19′)	3.861 [d]
O(5)–N(1)	1.288 [a]	O(6)–Mn–O(5)	89.7°
O(6)–N(2)	1.285 [a]	O(10)–Mn–O(11)	88.4°
O(7)–N(3)	1.291	O(6)–Mn–O(10)	91.7°
O(8)–N(4)	1.293	O(11)–Mn–O(5)	90.2°
Mn···Mn	13.583 (intrachain)	O(9)–Mn–O(12)	156.1°
Mn···Mn	9.308, 11.268, 11.539 (interchain)	O(5)–Mn–O(10)	178.4°
5			
Cu(1)–O(5)	2.418 [a] Å	O(7)···O(7′)	5.861 [b]
Cu(2)–O(6)	2.414 [a]	O(8)···O(8′)	6.015 [b]
Cu(1)–O(9)	1.931	O(8)···O(6′)	5.344 [c]
Cu(2)–O(10)	1.940	O(7)···C(6′)	3.828 [d]
		O(7)···C(7′)	4.110 [d]
O(5)–N(1)	1.289 [a] Å	O(7)···C(26′)	3.598 [d]
O(6)–N(2)	1.267 [a]	O(7)···C(28′)	4.265 [d]
O(7)–N(3)	1.280	O(8)···C(17′)	3.508 [d]
O(8)–N(4)	1.297	O(8)···C(19′)	3.658 [d]
Cu(1)···Cu(2)	13.780 (intrachain)	O(5)–Cu(1)–O(5)	180.0°
Cu(1)···Cu(1)	11.060 (interchain)	O(6)–Cu(2)–O(6)′	180.0°
Cu(2)···Cu(2)	11.060 (interchain)	O(5)–Cu(1)–O(9)	93.4°
Cu(1)···Cu(2)	11.648 (interchain)	O(5)–Cu(1)–O(9)′	86.6°
		O(5)–Cu(1)–O(10)	94.5°
		O(5)–Cu(1)–O(10)′	85.5°
		O(6)–Cu(2)–O(12)	96.8°
		O(6)–Cu(2)–O(12)′	83.2°
		O(6)–Cu(2)–O(11)	90.1°
		O(6)–Cu(2)–O(11)′	89.9°

[a] Coordination site.
[b] Closest TEMPO–TEMPO nitroxide contacts between uncoordinated sites on different chains.
[c] Indicates a contact between an uncoordinated TEMPO nitroxide oxygen and a coordinated TEMPO nitroxide oxygen.
[d] Indicates a likely O···(H)C hydrogen-bond like contact.

could also act as a source of the through-space interactions that will be proposed below.

3.2. Magnetism

The Curie–Weiss plot of $1/\chi$ versus T for **4** (Fig. 5) is essentially linear, with slope $C = 2.776$ emu-K/Oe-mol and Weiss constant $\theta = -0.35$ K. The χT versus T plot is relatively level at higher temperatures, but decreases significantly below 10 K, showing the onset of antiferromagnetic (AFM) interactions.

The best model to fit the magnetic results assumes that the two nitroxide units coordinated with the manganese ion are strongly and antiferromagnetically exchange coupled to give a TEMPO–Mn–TEMPO unit with net spin $S = (5/2)–(1/2)–(1/2) = (3/2)$, while the two uncoordinated nitroxide units act as independent $S = (1/2)$ units. For such a system, the Curie constant C is given by Eq. (1),

$$C = \frac{N\mu_B^2}{3k} \times [g_{rad}^2 S_{rad}(S_{rad}+1) + g_{eff}^2 S_{eff}(S_{eff}+1) + g_{rad}^2 S_{rad}(S_{rad}+1)] \quad (1)$$

where g_{rad} and g_{eff} are the g-factors for the isolated nitroxide and TEMPO–Mn–TEMPO units, respectively; S_{rad} and S_{eff} are the spin quantum numbers for the same units. For $S_{rad} = 1/2$ and $S_{eff} = 3/2$ with $g_{rad} = 2.007$ (from ESR for a nitroxide unit), setting $g_{eff} = 2.070$ yields $C = 2.77$ emu-K/Oe-mol in good agreement with the experimental Curie constant.

As additional confirmation of this model for the magnetic behavior of **4**, we analyzed the magnetization versus field behavior at 1.8 K (M versus H, Fig. 5b). The magnetization for a sum of one $S = 3/2$ plus two $S = 1/2$ spin sites is given by Eq. (2)

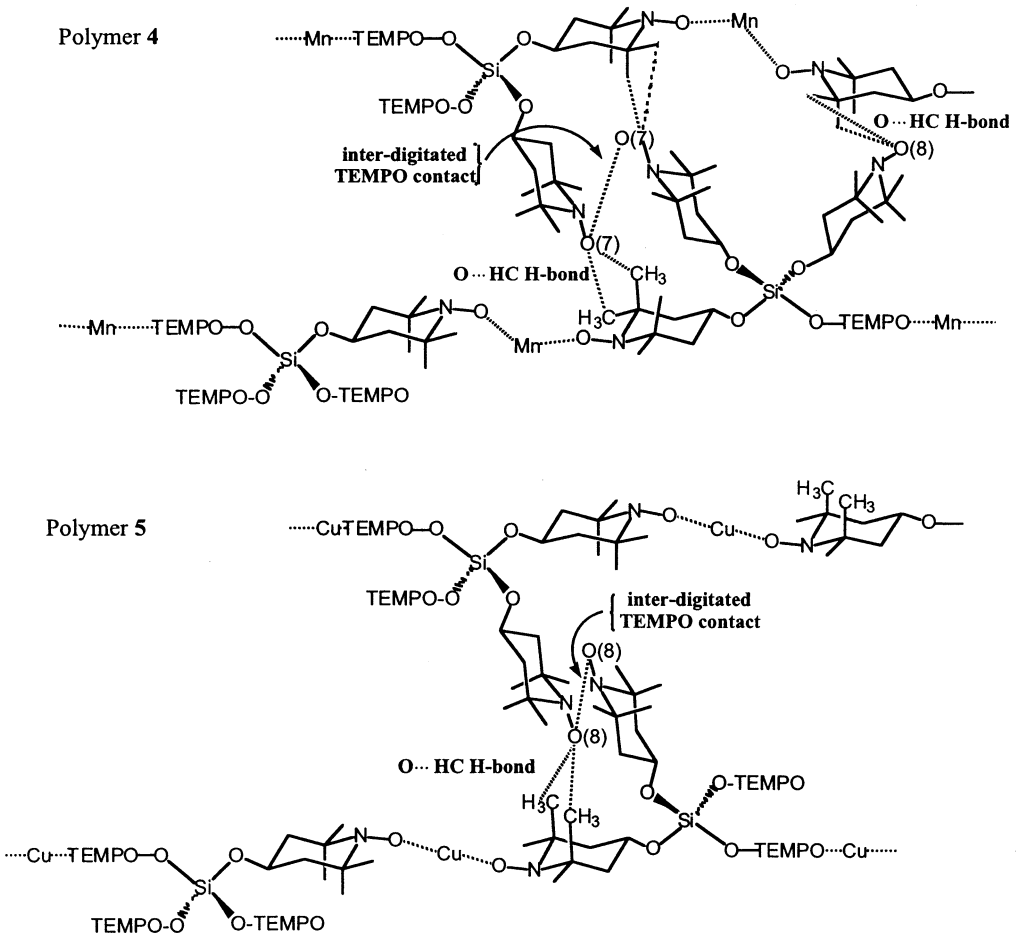

Fig. 7. Schematic representation of interchain contacts in **4** and **5**.

$$M = N\mu_B[g_{rad}S_{rad}B_{rad}(\eta_{rad}) + g_{eff}S_{eff}B_{eff}(\eta_{eff}) + g_{rad}S_{rad}B_{rad}(\eta_{rad})] \quad (2)$$

where $\eta_i = g_i\mu_B H/k(T-\theta)$ in which g_{rad} is the g-value for the isolated TEMPO sites, g_{eff} is a net g-value for the TEMPO–Mn–TEMPO unit, $g_i = g_{rad}$ or g_{eff}, 0 is a mean field correction, and B_{rad}/B_{eff} are Brillouin functions. Fixing $g_{rad} = 2.007$ as above, the best fit to the data gives $g_{eff} = 2.327$ and $\theta = -0.77$ K. The high field value of M in Fig. 5b approaches 5 μ_B/mol, as expected for a system containing one $S = 3/2$ plus two $S = 1/2$ spin units. Although g_{eff} is a bit larger than estimated by Eq. (1), the value is still reasonable for the model. The M versus H data at 3 K also fits this model well.

Mn(II) coordinates with nitroxides in either axial or equatorial coordination to give a $S = 3/2$ unit from TEMPO–Mn–TEMPO sites in **4** coupled through strong AFM exchange interactions.[8] But, the exchange coupling *between* the trimer spin units of **4** is not large. It is not clear whether the decrease in χT at < 10 K is due to AFM exchange across a bonded [Mn(TEMPO)–OSiO–[Mn(TEMPO)] sequence within the chain, or to some sort of through-space intermolecular spin pairing. As mentioned above, the closest approaches between uncoordinated TEMPO nitroxide groups are $r(NO\cdots ON) = 5.9$–6.0 Å; there are somewhat closer approaches between uncomplexed and complexed TEMPO groups in both **4**–**5** that may give through-space interactions. The direct distances between manganese ions are > 9 Å. So, direct through space exchange between spin-bearing groups on different chains of **4** should be weak, as observed. But, through-bond exchange in **4** also should be weak, given the lack of a strongly spin-polarizing conjugation pathway. For this reason, we favor through-space spin pairing of TEMPO spins as the source of the AFM interaction at low temperature in **4**, possibly via a spin-polarization mechanism involving the close contacts N–O sites and TEMPO methyl groups (see Table 3). The possibility of dipolar interactions between spin units—although expected to be weaker—should not be disregarded.

Cu(II) is known to give FM exchange coupling with TEMPO in axial coordination [8,9]. Based upon the geometry of **5**, the TEMPO–Cu–TEMPO unit would form an $S = 3/2$ unit, and the magnetic behavior would resemble that of **4** if the uncoordinated TEMPO units acted as isolated $S = 1/2$ units. Indeed, this is the behavior observed although the temperature depen-

dence of χT is somewhat different from that of **4**. The Curie–Weiss plot of Fig. 6a yields a slope of $C = 2.105$ emu-K/Oe-mol and Weiss constant of $\theta = -0.8$ K (extrapolated from the $T > 100$ K data). The value of the Curie constant is smaller than expected from Eq. (1), assuming $S_{rad} = 1/2$ and $S_{eff} = 3/2$. χT versus T rises to a maximum of 2.3 emu-K/Oe-mol as temperature drops to 18 K and finally decreases to about 1.2 emu-K/Oe-mol by 1.8 K (Fig. 6a). Apparently, the TEMPO–Cu–TEMPO units are FM exchange coupled, but more weakly than the TEMPO–Mn–TEMPO units in **4**. At lower temperatures, the onset of AFM exchange mechanisms causes a downturn in the plot.

The χT data for **5** were fit to Eq. (3) accounting for FM interaction of three $S = 1/2$ units in the TEMPO–Cu–TEMPO moiety, plus two independent $S = 1/2$ units for the non-coordinated TEMPO units. The exchange constant within the TEMPO–Cu–TEMPO unit is J/k, while g_{rad} and g_{eff} have meanings analogous to those given for Eq. (2) above. $C_{S=1/2}$ is the Curie law expression for χT in an $S = 1/2$ unit (see the earlier discussion of complex **4**). For the fitting, $g_{rad} = 2.00$ was fixed, while J/k, g_{eff}, and TIC were optimized.

$$\chi T = \chi T_{trimer} + 2C_{S=1/2} + \mathrm{TIC} \tag{3}$$

where

$$\chi T_{trimer} = \frac{N\mu_B^2 g^2}{4k} \frac{[10\exp(J/kT) + \exp(-2J/kT) + 1]}{[2\exp(J/kT) + \exp(-2J/kT) + 1]},$$

and TIC accounts for temperature independent contributions such as diamagnetism.

Fig. 6b shows the fit of the data to Eq. (3), down to the maximum in χT. The fit is quite reasonable, yielding $g_{eff} = 2.18$, $J/k = 89$ K. This value is somewhat imprecise due to the interference of the lower temperature AFM mechanism that has not been introduced in the fit, but clearly shows that the Cu–TEMPO interactions in **5** are ferromagnetic and significantly weaker than the Mn–TEMPO interactions in **4**.

We presume that the low temperature AFM interaction in **5** comes from close contacts between the uncoordinated TEMPO groups, again possibly by a spin polarization pathway involving the NO group of one TEMPO with methyl groups on a TEMPO in another chain (Table 3). In principle, the low temperature effects could derive from interaction within a TETRA cluster (intramolecular TEMPO–TEMPO exchange), but the large distances between nitroxide spin sites would seem to favor interchain interaction for this effect. We have insufficient direct evidence to prove these suggested magneto-structural mechanisms at this point, so further studies would be needed to clarify the magnetic behavior of **5**.

4. Conclusions

The formation of 2-D and 3-D nets from coordination of polyradicals with paramagnetic cations is not straightforward, even when topologically plausible. The use of silicon as a central atom in the tetraradical portion of systems offers more potential than use of carbon, because of the opportunity for d-orbital participation in the exchange routes. Despite the disadvantages of tetraradical **3** as an exchange linker (no direct conjugation paths across the molecule), it does yield structurally promising polymeric 1-D chains in coordination with metal cations. The coordination between paramagnetic cation and nitroxide yields strong TEMPO–metal exchange interactions, as desired, and in qualitative accord with the nature of exchange in related systems. However, only weak AFM interactions between spin units are observed at low temperature, which can be attributed to intermolecular interaction between spin sites. Future work will involve varying the spin carrier unit to change the geometry of the tetraradical, hopefully rendering the formation of higher dimensional nets easier. We also continue to seek better intramolecular exchange strategies to link radical spins through central d-orbital containing atoms, using tetraradicals such **1**.

5. Supplementary material

Supplementary material includes CIF files and crystallographic summary data (http://www.chem.umass.edu/~lahti/xray). CIF files for **3**-α, **3**-β, **4**, and **5** are Cambridge Crystallographic Databank as deposition numbers 172624,[2] 204385, 204386 and 204387, respectively.

Acknowledgements

This work was supported by the National Science Foundation (CHE 9809548 and CHE 0109094), the Comision Interministerial de Ciencia y Tecnologia (CICYT-MAT2000-1388-C03-03), and the Fullbright España Comision. We thank G. Dabkowski of the UMass-Amherst Microanalytical Laboratory for elemental analyses. Magnetic measurements for **5** were obtained at the UMass-Amherst Nanomagnetics Characterization Facility (NSF CTS-0116498).

References

[1] For examples of the strategy of making hybrid organic/inorganic nets with organic nitroxides and polynitroxides, see:(a) K. Inoue, T. Hayamizu, H. Iwamura, Mol. Cryst. Liq. Cryst. Sci. Technol.,

Sect. A 273 (1995) 505.
(b) H. Iwamura, K. Inoue, T. Hayamizu, Pure Appl. Chem. 68 (1996) 243.
[2] Y. Liao, M. Baskett, P.M. Lahti, F. Palacio, Chem. Commun. (2002) 252–253.
[3] F. Mathevet, D. Luneau, J. Am. Chem. Soc. 123 (2001) 7465–7466.
[4] (a) E.G. Rozantsev, V.A. Golubev, Izv. Akad. Nauk. SSSR. Ser. Khim. 3 (1965) 548;
(b) P.W. Kopf, R.W. Kreilick, D.G.B. Boocock, E.F. Ullman, J. Am. Chem. Soc. 92 (1970) 4531;
(c) A. Nakajima, H. Ohya-Nishiguchi, Y. Deguchi, Bull. Chem. Soc. Jpn. 44 (1971) 2120;
(d) E.A. Gruzinova, A.K. Litkovetz, E.V. Gruzinov, Russ. Chem. Bull. 44 (1995) 956.
[5] We have also attempted complexation with $Co(hfac)_2$ and $Ni(hfac)_2$. Preliminary results again indicate the formation of 1:1 complexes as 1-D chains.
[6] G.M. Sheldrick, SHELXL-97, Program for the Refinement of Crystal Structure, University of Göttingen, Germany.
[7] For an example of a $Mn(hfac)_2$-TEMPO coordinated system, see: P. Jaitner, W. Huber, G. Huttner, O. Scheidsteger, J. Organomet. Chem. 259 (1983) C1 (Cambridge Structure Databank Code CAVLIU). For an example of a hexacoordinate $Cu(hfac)_2$-TEMPO system, see O.P. Anderson, T.C. Keuchler, Inorg. Chem. 19 (1980) 1417 (Cambridge Structure Databank Code FAPOCU).
[8] See for example the following discussions:(a) A. Caneschi, D. Gatteschi, R. Sessoli, In: D. Gatteschi, O. Kahn, J.S. Miller, F. Palacio, (Eds.), Magnetic Molecular Materials, Kluwer: Dordrecht, The Netherlands, 1991, p. 215 and references therein;
(b) D. Gatteschi, P. Rey, In: P.M. Lahti (Ed.), Magnetic Properties of Organic Materials, Marcel Dekker, New York, NY, 1999, p. 601ff.
[9] To give just one example, in: K. Giesar, W. Haase, I. Svoboda, H. Fuess, Inorg. Chim. Acta, 287 (1999) 181, g(Cu—NIT) = 2.06 for Cu–TEMPO derivatives.